Published in final edited form as:
Biochemistry. 2011 March 29; 50(12): 2371–2380. doi:10.1021/bi101568j.

Local and Global Dynamics of the G Protein-Coupled Receptor CXCR1

Sang Ho Park, **Fabio Casagrande**, **Bibhuti B. Das**, **Lauren Albrecht**, **Mignon Chu**, and **Stanley J. Opella***
Department of Chemistry and Biochemistry, University of California, San Diego, 9500 Gilman Drive, La Jolla, California 92093-0307, USA

Abstract

The local and global dynamics of the chemokine receptor CXCR1 are characterized using a combination of solution NMR and solid-state NMR experiments. In isotropic bicelles (q=0.1), only 13% of the expected number of backbone amide resonances is observed in $^{1}H/^{15}N$ HSQC solution NMR spectra of uniformly ^{15}N labeled samples; extensive deuteration and the use of TROSY made little difference in the 800 MHz spectra. The limited number of observed amide signals are ascribed to mobile backbone sites, and assigned to specific residues in the protein; nineteen of the signals are from residues at the N-terminus and twenty-five from residues at the C-terminus. The solution NMR spectra display no evidence of local backbone motions from residues in the trans-membrane helices or inter-helical loops of CXCR1. This finding is reinforced by comparisons of solid-state NMR spectra of both magnetically aligned and unoriented bilayers containing either full-length or doubly N- and C-terminal truncated CXCR1 constructs. CXCR1 undergoes rapid rotational diffusion about the normal of liquid crystalline phospholipid bilayers; reductions in the frequency span and a change to axial symmetry are observed for both carbonyl carbon and amide nitrogen chemical shift powder patterns of unoriented samples containing ^{13}C and ^{15}N labeled CXCR1. In contrast, when the phospholipids are in the gel phase, CXCR1 does not undergo rapid global reorientation on the 10^4 Hz timescale defined by the carbonyl carbon and amide nitrogen chemical shift powder patterns.

Keywords

solid-state NMR; membrane bilayers; chemical shift anisotropy; rotational diffusion; protein dynamics; GPCR

Local and global motions are essential properties of proteins, since they strongly influence their structures, interactions, and functions. In general, the dynamics of membrane proteins (1-7) are not as well characterized as those for water-soluble globular proteins (8), largely due to difficulties encountered in the expression, purification, and refolding of membrane proteins into uniform, active samples, as well as the limitations of current experimental methods and instrumentation. NMR spectroscopy is sensitive to a wide range of amplitudes and frequencies of motions, and it is a fundamentally sound approach to characterizing protein dynamics in almost any situation, including protein-containing micelles, bicelles (9, 10), and bilayers. Here we describe the results of a combination of experiments on that apply solution NMR to protein-containing isotropic bicelle samples and both oriented sample (OS)

*Contact information for the corresponding author, Stanley J. Opella: sopella@ucsd.edu, Phone: 858 822-4820, FAX: 858 822-4821.

Supporting Information **Available**: Sequence of CXCR1 constructs, comparison of solution NMR spectra of CXCR1 constructs, and NMR resonance assignment table of CXCR1. This material is available free of charge via the Internet at http://pubs.acs.org.

and magic angle spinning (11) solid-state NMR to aligned and unoriented phospholipid bilayer samples. This approach characterizes the local backbone and global motions of the 350-residue G protein-coupled receptor (GPCR) CXCR1. Because results obtained on CXCR1 in phospholipid bilayers are included, these findings complement the structure determination of this protein in its native, functional environment of planar phospholipid bilayers under physiological conditions by solid-state NMR spectroscopy (12).

Although NMR studies of membrane protein dynamics are still at an early stage of their development, it is established that the chemically, physically, and dynamically asymmetric liquid crystalline bilayer environment in which they reside has a profound effect on their structure and dynamics. This is reflected in the two major classes of motions found in the initial studies of CXCR1: (1) there are local rapid backbone motions of residues near the N- and C- termini of the protein in all lipid environments examined; and (2) the protein undergoes rapid global rotational diffusion about the normal of liquid crystalline phospholipid bilayers.

These motions are of direct relevance to the structure and function of CXCR1. The chemokine interleukin-8 (IL-8), the natural ligand of CXCR1, has been shown to bind to residues near the N-terminus of the receptor (13, 14); these residues are unstructured and mobile in the absence of the ligand. In response to inflammatory stimuli, CXCR1 mediates cell migration and activation of polymorphonuclear neutrophils (PMN) (15, 16) and IL-8 induced chemotaxis that requires global motions of the receptor to direct the PMN to sites of inflammation where IL-8 is secreted by macrophages, lymphocytes, and epithelial and endothelial cells. Clearly, the interactions of amino acid residues of IL-8 with those of CXCR1 are directly relevant to the mechanisms of actions of its biological functions, and the motions of the N-terminal residues of CXCR1 undoubtedly affect these interactions.

The experimental studies are correlated with the primary structure CXCR1 by Figure 1, which shows the amino acid sequence of full-length human CXCR1 arranged schematically so that it suggests the locations of the seven trans-membrane helices, inter-helical loops, and terminal regions that constitute the main elements of the protein (17). The blue (N-terminus) and red (C-terminus) colors designate the residues found to undergo rapid local backbone motions by NMR spectroscopy; only terminal residues are observed to undergo motions on the relevant NMR timescales ($\geq 10^4$ Hz).

Materials and Methods

Expression of CXCR1 constructs

Isotopically labelled samples of wild-type full-length CXCR1 ($WT_{1\text{-}350}$) and five truncated CXCR1 constructs were prepared for the NMR experiments, including N-terminal truncated CXCR1 ($NT_{39\text{-}350}$), C-terminal truncated CXCR1 ($CT_{1\text{-}319}$), doubly N- and C-terminal truncated CXCR1 ($DT_{23\text{-}319}$), C-terminal 3 transmembrane CXCR1 ($3TM_{193\text{-}350}$), and the N-terminal domain of CXCR1 ($ND_{1\text{-}38}$). The DNA sequences corresponding to each of the truncated constructs were sub cloned from that previously described for full-length CXCR1 ($WT_{1\text{-}350}$) construct (pGEX2a-CXCR1-6His) (12). The DNA sequences were PCR amplified using the corresponding primers and pGEX2a-CXCR1-6His as template DNA. The amplified genes were ligated back into the pGEX2a plasmid (Amersham Pharmacia, www.gelifesciences.com) after digestion with *BamHI* and *SmaI*, and purification by agarose gel electrophoresis. Proteins expressed in pGEX2a are under control of the *pTac* promoter and carry an N-terminal glutathione S-transferase (GST) fusion protein that can be removed by utilizing the included thrombin cleavage site. The DNA for all of the constructs was verified by sequencing. Heterologous expression of uniformly and selectively isotopically labelled CXCR1 constructs in *E. coli* was performed in M9 minimal media. Optimal

expression was obtained with *E. coli* BL21 (DE3) for the 38-residue N-terminal domain, ND_{1-38}, and with *E. coli* BL21 for the truncated CXCR1 constructs. Uniformly 35% ^{13}C, 100% ^{15}N labeled full-length CXCR1 (WT_{1-350}) was expressed in specially prepared BioExpress growth media obtained from Cambridge Isotope laboratories (www.isotope.com).

Purification and refolding

The polypeptides corresponding to NT_{39-350}, CT_{1-319}, DT_{23-319}, and $3TM_{193-350}$ were purified and refolded following the protocol previously described for the full-length CXCR1 (WT_{1-350}) receptor (12). The inclusion bodies of the GST-fused receptor constructs resulting from a 1liter bacterial culture were solubilized in 30 ml binding buffer (1% SDS, 20 mM Tris-HCl, 300 mM NaCl, 5 mM TCEP, pH 7.5). The solution was filtered with Steriflip 0.22 ⌠m filter devices (Millipore, www.millipore.com), and subjected to immobilized metal ion affinity chromatography (Ni-NTA superflow, Qiagen, www.qiagen.com). The column was washed with five bed volumes of binding buffer and 10 bed volumes of thrombin cleavage buffer (TCB: 0.1% hexadecylphosphocholine (Anatrace, www.affymetrix.com), 20 mM Tris-HCl, 200 mM NaCl, pH 8.0). 1000 units of thrombin in 20 ml TCB were loaded onto the column to cleave the GST-fusion proteins under gentle agitation over night at room temperature. After removal of GST, the proteins were washed with 10 bed volumes of washing buffer (0.5% dodecylphosphocholine (Anatrace), 20 mM Tris-HCl, 300 mM NaCl, 10 mM imidazole, pH 8.0). Finally, the proteins were eluted with elution buffer (washing buffer with 400 mM of imidazole). Size exclusion chromatography was subsequently used in order to obtain samples that contained only monomers of the CXCR1 constructs. Refolding was performed as previously described by reconstitution of the proteins into mixtures of DMPC and POPC lipids. Dialysis against solutions containing methyl-β-cyclodextrin removed the detergents (18, 19), generating pure proteoliposome pellets after centrifugation.

For the N-terminal domain alone, ND_{1-38}, two different purification protocols were utilized, since the GST-fused ND_{1-38} was found to be present in both IBs and the soluble cytosolic fraction of *E. coli* BL21 (DE3) cells following expression. IBs of ND_{1-38} were purified as described above using higher concentrations of imidazole in the binding (30 mM) and wash (40 mM) buffers. Since ND_{1-38} is soluble in aqueous buffer after removal of GST, no detergent was used in the wash and elution buffers. After collecting the IBs by centrifugation at 40,000 g for 45 min at 15°C, the cytosolic GST-fused ND_{1-38} fraction in the supernatant was filtered (0.22 ⌠m) and purified by Ni-NTA chromatography, also without the use of detergents. Soluble ND_{1-38} was dialyzed against nanopure water for two days at room temperature, and then lyophilized for storage.

NMR sample preparation

All NMR samples of the CXCR1 constructs, except for the soluble ND_{1-38} polypeptide, were prepared from proteoliposome pellets (20% wt lipid) in which 1 mg of the CXCR1 construct was reconstituted in 10 mg of a DMPC/POPC (8:2, w/w) lipid mixture.

The protein-containing isotropic bicelle samples (q=0.1) used in the solution NMR experiments were prepared by dissolving 1 mg of the CXCR1 construct-containing proteoliposome pellets in 400 μl of 360 mM perdeuterated DHPC (Cambridge Isotope Laboratories), solution containing 10% (v/v) ^2H_2O, at pH 4.0. The ND_{1-38} samples were prepared by dissolving the lyophilized polypeptide directly into preformed isotropic bicelles.

The unoriented phospholipid bilayer samples were prepared by ultracentrifugation of 2-3 mg of CXCR1 construct in a proteoliposome pellet at 300,000 g for 2 hrs at 15°C, then the

centrifuged pellet was transferred either to a flat-bottom 5 mm outer diameter glass tube (New Era Enterprises, newera-spectro.com) for stationary solid-state NMR experiments or to a 3.2 mm OD rotor for MAS solid-state NMR experiments.

The magnetically aligned protein-containing bilayer samples were prepared by adding an aqueous solution containing the short chain lipid, DHPC, to 3 mg of a CXCR1 construct in a proteoliposome pellet. The translucent proteoliposome pellet turns into a clear, non-viscous solution when placed on ice, which is strongly indicative of the formation of a magnetically-alignable bilayer phase (20).

The q=3.2 samples had a lipid concentration of 28% (w/v), and contained 300 mM long chain lipids in a volume of 200 μl at pH 7.3. For the OS solid-state NMR experiments, a flat-bottom 5mm NMR tube was filled with 180 μl of the solution, and the tube was sealed with a rubber cap that formed a tight seal

NMR experiments

Solution NMR experiments were performed at 50°C on Varian VS 800 MHz and Bruker DRX 600 MHz spectrometers equipped with 5 mm triple-resonance cold probes and z-axis gradients. Heteronuclear solution NMR experiments were performed on uniformly ^{15}N-labeled or uniformly ^{13}C/^{15}N-double-labeled samples in q=0.1 isotropic bicelles with a protein concentration of 50 μM. These experiments included the standard two-dimensional ^{1}H-^{15}N HSQC (21), three-dimensional ^{15}N-edited NOESY-HSQC (22) with mixing time of 200 ms, and three-dimensional HNCA and HNCOCA (23).

The solid-state ^{13}C NMR spectra of unoriented samples of 35% randomly ^{13}C and 100% uniformly ^{15}N labeled CXCR1 in phospholipid bilayers were obtained on a 750 MHz Bruker Avance spectrometer equipped with a 3.2 mm triple-resonance MAS probe. The spectrometer was operated at resonance frequencies 749.041 and 188.379 MHz for ^{1}H and ^{13}C, respectively. Experiments were carried out either without spinning (stationary) or with relatively slow magic angle spinning at 5 kHz. MOISTCP (24) and CPMAS pulse sequences were used to acquire one-dimensional stationary and MAS spectra, respectively. During cross polarization, typically a 60 kHz radio frequency field was applied during MOIST cross-polarization, and a ramped RF amplitude modulation was applied to the ^{1}H irradiation in the MAS experiments. A 1 ms contact time was used for most cross-polarization experiments. An 80 kHz RF field was used with SPINAL-16 composite decoupling (25) on the ^{1}H channel during data acquisition. The one-dimensional spectra resulted from signal averaging 1000 or 2000 transients with a 3 s recycle delay at low or high temperatures, respectively. An exponential function corresponding to 300 Hz of line broadening was applied to the free induction decays prior to Fourier transformation. Two-dimensional chemical shift anisotropy (CSA) recoupling was performed with the SUPER pulse sequence (26) with the 5 kHz MAS spinning stabilized to ±2 Hz. Taking into account the theoretical scaling factor of 0.155, the total spectral width in the indirect dimension was 32.258 kHz. SPINAL-16 decoupling with a 90 kHz RF field was applied on the ^{1}H channel during the CSA evolution. 60.6 kHz RF fields were used for cross-polarization and recoupling pulses during evolution in t_1. 2000 scans were signal averaged for each of 16 t_1 complex points with a 3 s recycle delay. An exponential function corresponding to 300 Hz of line broadening was applied in the direct dimension, and a Lorentzian to Gaussian apodization function with a net line broadening of 35 Hz was applied in the indirect dimension. A zero-filled two-dimensional data matrix of 2048×128 points was Fourier transformed and processed with the hyper complex method (STATES-TPPI) (27). The sample temperature was measured under both stationary and MAS spinning conditions by observing the chemical shift difference between the two ^{1}H resonances in a methanol sample (28). Simulations were carried out using the SIMPSON software package (29).

The solid-state ^{15}N NMR spectra were obtained on a 700 MHz Bruker Avance spectrometer. The homebuilt $^{1}H/^{15}N$ double-resonance probe used in the experiments had 5 mm inner diameter solenoid coil tuned to the ^{15}N frequency and an outer MAGC “low E” coil tuned to the ^{1}H frequency (30). The one-dimensional ^{15}N NMR spectra were obtained by cross-polarization with a contact time of 1 ms, a recycle delay of 6 s, and an acquisition time of 10 ms. For each spectrum, between 1024 and 8096 transients were signal averaged for each spectrum, and an exponential function corresponding to line broadening of 50 Hz - 100 Hz was applied to each free induction decay prior to Fourier transformation. The NMR data were processed using the programs NMRPipe/NMRDraw (31). The chemical shift frequencies were externally referenced to ^{15}N-labeled solid ammonium sulfate, defined as 26.8 ppm, which corresponds to the signal from liquid ammonia at 0 ppm.

Results

Local backbone dynamics of CXCR1 in isotropic bicelles

Solution NMR experimental methods and instrumentation can be used to study small membrane proteins in highly optimized micelle and isotropic bicelle environments. However, with a few notable exceptions (32, 33), applications of solution NMR to membrane proteins with more than three or four transmembrane helices are generally limited by the slow overall reorientation rates of the protein-lipid aggregates, which result in broad line widths of the protein resonances, and correspondingly poor resolution and sensitivity. However, it is possible to observe some resonances with relatively narrow line widths and correspondingly higher intensities from those residues that undergo substantial local backbone motions in solution NMR spectra of larger membrane proteins, including GPCRs, such as rhodopsin (34), the vasopressin V_2 receptor (35) solubilized with detergents, and as we demonstrate here CXCR1 in isotropic bicelles.

We utilized standard two-dimensional $^{1}H/^{15}N$ HSQC solution NMR experiments to observe signals from only those residues undergoing significant local motions in full-length CXCR1. The spectra in Figure 2 are from samples of uniformly and selectively ^{15}N labeled full-length CXCR1 ($WT_{1\text{-}350}$) in isotropic bicelles (q=0.1). Notably, only 44 (out of 350) resonances are observed in the spectrum of uniformly ^{15}N-labeled full-length CXCR1 in Figure 2A. The vast majority of protein resonances are not present in solution NMR spectra because the structured residues in the trans-membrane helices and the inter-helical loops are too broad to be observed under these experimental conditions. Few differences are observed between the standard HSQC spectrum in Figure 2A and an 800 MHz TROSY(36) spectrum obtained on a sample where approximately 80% of the hydrogens bonded to carbons were replaced by deuterons. The only noticeable difference was that the line widths of the observed subset of resonances were slightly narrower (Figure S1) than those in Figure 2A. Notably, only a few additional signals were apparent in the TROSY spectrum, demonstrating that the combination of a relatively high level of deuteration and TROSY at 800 MHz was unable to narrow the resonances associated with residues in the helices and inter-helical loops in q=0.1 bicelles sufficiently for detection on a solution NMR spectrometer. Significantly, all of the resonances observed in Figure 2A, which are assigned to mobile N- and C-terminal residues, disappear when the sample is transferred to a solution that is predominantly D_2O instead of H_2O (data not shown). This demonstrates that all of the amide sites that contribute observable resonances in Figure 2A undergo rapid solvent exchange, which is consistent with their being mobile, solvent exposed residues. The signals in Figure 2A were assigned to specific residues located at the N- and C- termini of full-length CXCR1 by comparisons among spectra obtained from selectively ^{15}N labeled (by residue type) samples and from uniformly ^{15}N labeled truncated constructs.

These data were supplemented with the results of triple-resonance backbone assignment experiments on uniformly ^{13}C and ^{15}N labeled samples of CXCR1.

The two-dimensional HSQC spectra in Figure 2 from several selectively ^{15}N labeled samples provide residue-type assignments of resonances that serve as anchor points for sequential resonance assignments. However, simply by counting the number of observable signals for each type of labeled amino acid, and comparing that to the distribution of amino acids at the N- and C- termini of CXCR1 (Figure 1), most of the mobile terminal residues can be identified. For example, there are only four distinct signals (three strong signals and one weak signal with low contour level processing) from the selectively ^{15}N-valine labeled sample (Figure 2C and Figure S2). There are thirty valine residues in the full-length CXCR1 sequence (Figure 1); significantly, only four of the valine residues are located near the C-terminus (residues 326, 336, 344, and 346) and none near the N-terminus. Three signals are observed in the spectrum and their assignments noted. These data suggest that valine 326 is restrained by the secondary and/or tertiary structure of the protein, but ten residues away, valine 336 has sufficient local motions to be detected in the solution NMR spectrum. Similarly, the selective labeling with ^{15}N glycine and serine (Figure 2B) and ^{15}N methionine (Figure 2D) demonstrates that there are mobile residues at the N-terminus of the protein. All of the observable resonances are reiterated in the composite “dot” spectrum in Figure 3E where there are a total of eighteen blue dots from mobile N-terminal residues and twenty five red dots. Two- and three-dimensional NOE experiments, triple-resonance HNCA and HNCOCA, and comparisons of spectra of various truncated CXCR1 constructs (Figure 3) provided the sequential resonance assignments listed in Table S1. This information served to delineate the boundaries of the mobile terminal residues in the sequence, as denoted in Figure 1 by the red and blue regions at the termini.

The spectra in Figure 3 from the truncated constructs of CXCR1 also demonstrate that only N- and C-terminal residues are mobile. As expected in Figure 3B and F only resonances assigned to C-terminal residues are present, since the protein is missing residues 1 - 38 at the N-terminus of the construct $NT_{39\text{-}350}$. Notably, the ^{1}H and ^{15}N chemical shift frequencies of the red dots representing these resonances in Figure 3E and F are the same, demonstrating that the N-terminal residues do not affect the C-terminal residues of CXCR1. The same conclusion is reached from the spectrum of the C-terminal truncated construct $CT_{1\text{-}319}$ (Figure 3C and G) where the resonances from the mobile N-terminal residues have the same chemical shift frequencies as the corresponding residues in the full-length protein $WT_{1\text{-}350}$ (Figure 3A and E).

The N-terminal domain of CXCR ($ND_{1\text{-}38}$) is soluble in water, and its experimental spectrum in Figure 3D contains resonances from all of its residues, with the same narrow ^{1}H chemical shift dispersion of about 1 ppm observed in the spectra of the larger CXCR1 constructs. The eighteen signals assigned to mobile N-terminal residues in the spectra of the full-length ($WT_{1\text{-}350}$) and C-terminal truncated ($CT_{1\text{-}319}$) CXCR1 constructs have in this 38-residue polypeptide, suggesting that these residues are mobile, unstructured, and do not interact with the rest of the protein.

The results in Figures 2 and 3 along with the sequential resonance assignments (Table S1) show that a limited number of N-terminal residues and a larger number of C-terminal residues are mobile, and that there is no evidence of mobility from residues in the trans-membrane helices or inter-helical loops.

Rotational diffusion of CXCR1 in lipid bilayers

As first shown by Griffin and coworkers (37) with ^{13}C-carbonyl labeled bacteriorhodopsin, the characteristic motional averaging of the carbonyl chemical shift powder pattern from its

static asymmetric pattern with a large 155 ppm frequency span (Figure 4F) to a much narrower axially symmetric pattern (Figure 4A) can be used to demonstrate that a helical membrane protein undergoes rapid rotational diffusion about the bilayer normal at temperatures above that of the lipid phase transition. This is shown to be the case for CXCR1 in phospholipid bilayer samples using solid-state ^{13}C NMR experiments in the presence and absence of magic angle spinning. The experimental data shown in Figure 4 were obtained from an unoriented, ultracentrifuged proteoliposome pellet containing 35% randomly ^{13}C and 100% uniformly ^{15}N labeled full-length CXCR1 (WT_{1-350}). The ^{13}C labeling was at the diluted 35% level in order to minimize broadening and distortions due to ^{13}C-^{13}C homonuclear dipole-dipole interactions in the spectra of stationary samples. The same samples were used for the MAS solid-state NMR experiments, although the dilution was unnecessary in this situation because the magic angle spinning is sufficient to average out the effects of the homonuclear ^{13}C-^{13}C interactions. The simulated and experimental spectra in the top row of Figure 4 correspond to the CXCR1-containing proteoliposomes at 30°C and those in the bottom row at 5°C. In all cases, a significant difference can be observed in the carbonyl ^{13}C chemical shift powder pattern between the high temperature spectra (30°C) and the low temperature spectra (5°C), which corresponds to the phospholipids being in the liquid crystalline phase at 30°C and in the gel phase at 5°C.

The spectra in Figure 4D and I result from the simplest experiment, which was to obtain ^{1}H decoupled ^{13}C NMR spectra of a stationary, unoriented bilayer sample at high (30°C) and low (5°C) temperatures. In the spectrum in Figure 4D, two quite broad but still distinguishable peaks are observed between about 100 ppm and 250 ppm; the intensity centered around 120 ppm is attributed to aromatic carbons, and the intensity of interest, centered at 175 ppm, comes mainly from the carbonyl carbons in the protein backbone. At the lower temperature (Figure 4I) these two peaks merge into one very broad region of signal intensity. Typically, the span of the carbonyl carbon chemical shift anisotropy in the protein backbone is about 155 ppm and that of the multiple types of aromatic carbons is approximately 250 ppm, however they overlap somewhat and are consistent with the bulk of the observed intensity occurring between about 100 ppm and 250 ppm.

Although the spectra in Figure 4D and I obtained on stationary samples show that there is a large reduction of the breadth of both the carbonyl carbon and aromatic carbon powder patterns upon raising the sample temperature from 5°C to 30°C, MAS solid-state NMR experiments provide a clearer demonstration of this effect because the signals from the carbonyl and aromatic carbons can be separated by the differences in their isotropic chemical shifts. Two fairly broad peaks are observed between 100 ppm and 250 ppm in the MAS solid-state ^{13}C NMR spectrum obtained at 30°C (Figure 4E); the breadth is expected in the presence of magic angle spinning because each peak results from the overlap of hundreds of ^{13}C sites with similar isotropic chemical shifts. Notably, even though the spinning rate is relatively slow at 5 kHz there are no spinning sidebands apparent in the spectrum obtained at 30°C, indicating a small span for the chemical shift anisotropy present at the higher temperature. In contrast, the MAS solid-state NMR spectrum in Figure 4J obtained on the same sample under identical conditions, except that the temperature was 5°C, has multiple sidebands flanking the isotropic center band from the carbonyl carbons, indicating a large span for their chemical shift anisotropy at the lower temperature. The results obtained by comparing the spectra in Figure 4D and I and those in Figure 4E and J are consistent in showing dramatic narrowing of the chemical shift tensors as a function of temperature.

Chemical shift powder patterns can be reconstructed from the intensities of spinning sidebands (8, 38). This is a powerful tool in solid-state NMR spectroscopy. The experimental spinning sideband intensities measured from the data in Figure 4J provided

input for the calculation of the underlying powder pattern (Figure 4G), and then through simulation the intensities for an 'ideal' set of spinning sidebands that would be expected from that powder pattern, also shown in Figure 4G. The high temperature MAS spectrum (Figure 4E) has no observable sidebands at the 5 kHz spinning frequency. This makes the comparison between the spectra in Figure 4J and 4E very useful as a qualitative indicator of the presence of rotational diffusion in a membrane protein: the protein is immobile on the NMR timescales at the low temperature and undergoes fast rotational diffusion on the NMR timescales at the high temperature. However the absence of spinning sidebands at the higher temperature makes it difficult to determine the actual breadth and shape of the motionally averaged chemical shift anisotropy powder pattern. Moreover, the sensitivity was found to be 3-4 times higher at 5°C than at 30°C, making it more difficult to characterize the details of the spectral changes resulting from the motional averaging. The estimated stationary and spinning spectra for the carbonyl carbon resonances at 30°C are shown in Figure 4B for comparison.

To obtain more accurate carbonyl carbon chemical shift powder patterns at both high and low temperatures, and to demonstrate the potential of this approach for analyzing resolved resonances in complex spectra obtained by MAS solid-state NMR, two-dimensional experiments that correlate an isotropic chemical shift frequency in the direct dimension with a recoupled chemical shift powder pattern in the indirect dimension were performed on the samples of CXCR1 in unoriented bilayers. In this example the isotropic frequency represents a large number of overlapping resonances, but since they are mostly in the trans-membrane helices they are representative of residues in the helices aligned roughly parallel to the bilayer normal. MAS solid-state NMR experiments were performed at a relatively high ^{13}C resonance frequency (188 MHz), the SUPER pulse sequence (26) was chosen because its relatively large spectral width is able to cover the span of ~150 ppm (~ 30 kHz) of the static carbonyl carbon chemical shift anisotropy powder pattern (39). The RF fields applied during recoupling of the chemical shift anisotropy in the indirect dimension are twelve times the spinning frequency, therefore an RF field strength of 60.6 kHz was used with the 5 kHz spinning frequency. A complication of the SUPER experiment is that the isotropic chemical shift evolution depends on the offset from the RF irradiation frequency; consequently, shearing is required during data processing. To avoid this complication, the RF irradiation was applied at the center (175 ppm) of the band of resonances from the carbonyl carbons. Consequently, the one-dimensional spectral slices from the indirect dimension of the experiment that are shown in Figure 4C and H were taken at 175 ppm in the direct isotropic chemical shift dimension spectrum; this minimizes distortion of the resulting powder pattern line shape from the offset dependence of the experiment. It also ensures that the experimental data represent powder patterns from only those carbonyl groups whose isotropic chemical shift is 175 ppm. The experiment was performed on the same sample at high and low temperatures, and the resulting powder patterns displayed quite different spans in the liquid crystalline bilayers at 30°C (~25 ppm) and in the gel phase bilayers at 5°C (~150 ppm).

As described above, the data presented in Figure 4 were obtained with several quite different NMR experiments. However, they are all consistent in showing a dramatic decrease in the span of the carbonyl carbon chemical shift powder pattern as a consequence of temperature-induced motional averaging. The simulated spectra in Figure 4 were calculated using the principal values of σ_{11} = 242 ppm, σ_{22} = 186 ppm, σ_{33} = 96 ppm, and the isotropic value of σ_{iso} = 174.6 ppm. The simulated spectra shown in Figure 4A and F had 200 Hz of added line broadening and those in Figure 4B and G had 3 kHz of line broadening to match the appearance of the corresponding experimental spectra. Comparisons between the experimental and simulated powder patterns are consistent with the motional averaging resulting from rapid axial diffusion of the protein (and the trans-membrane helices) about

the bilayer normal at 30°C, and the protein (and helices) not undergoing substantial global motions at 5°C. Of course all of the conclusions about motional averaging are relative to the relevant NMR timescale, which in the experiments resulting in the data in Figure 4 is derived from the frequency span of the carbonyl carbon chemical shift powder pattern at this field strength (~ 30 kHz); rotation faster than this frequency will result in motionally averaged powder patterns, and rotation slower than this frequency will yield static powder patterns.

A slower timescale is monitored by the experimental results shown in Figure 5, since they are focused on the ^{15}N amide chemical shift anisotropy, which typically has a span of about 170 ppm in an immobile polypeptide site, as illustrated in the simulated spectrum in Figure 5J, which corresponds to ~ 2.5 kHz at this field strength. However, the ^{15}N amide chemical shift powder pattern line shapes are generally less sensitive to axial diffusion about the bilayer normal because the principal axis of the ^{15}N amide tensor is approximately collinear with the N-H bonds parallel to the helix axes. In Figure 5, the ^{15}N amide chemical shift powder patterns of full-length CXCR1 (WT_{1-350}) and the doubly truncated construct (DT_{23-319}) CXCR1 in phospholipid bilayers are compared for experimental conditions where the protein is immobile (5°C) and undergoing fast rotational diffusion about the bilayer normal (30°C). The proteins are 100% uniformly ^{15}N labeled, but because proteins have no nitrogen sites directly bonded to another nitrogen, and the backbone amide sites of interest are separated by bonds from two carbons, there is no interference from ^{15}N/^{15}N homonuclear dipolar couplings in either stationary or spinning experiments. The solid-spectra ^{15}N NMR spectra obtained at 5°C (bottom row) are powder patterns with a chemical shift span of about 170 ppm, which is typical of an immobile ^{15}N backbone amide site in a protein. At 30°C (top row), a modest reduction of the span of the ^{15}N amide chemical shift anisotropy powder pattern for both full-length and doubly truncated CXCR1 constructs in liquid crystalline phospholipid bilayers is observed. In a sample of selectively ^{15}N-valine labeled full-length CXCR1 (WT_{1-350}), a larger reduction of the span of the power pattern is observed (data not shown) because two-thirds of the valine residues, excluding those in the mobile N-terminus, are predicted to be in the trans-membrane helices. In the case of the uniformly ^{15}N labeled samples only about half of the labeled sites are in the trans-membrane helices and the others distributed among the inter-helical loops, which are affected differently by rotational diffusion about the bilayer normal. Similarly, we have shown dramatic changes in both the span and sign of the axially symmetric ^{15}N powder patterns from single sites in specifically and selectively ^{15}N labeled membrane proteins under conditions where the proteins undergo rapid rotational diffusional motion about the bilayer normal (7).

Some simple solid-state NMR experiments enable a more detailed spectral analysis of the ^{15}N powder patterns from uniformly ^{15}N labeled samples. The spectra in Figure 5 were obtained with two sets of experimental parameters The spectra in Figure 5A, C, F, and H were obtained by ^{1}H to ^{15}N cross-polarization with a relatively long mix time (1 ms) to ensure that signals are present from ^{15}N amide sites with both strong and weak heteronuclear dipolar couplings, including signals near the isotropic chemical shift values (~120 ppm) that generally have small heteronuclear dipolar couplings, are observed. In contrast, the spectra (Figure 5B, D, G, and I) obtained with a short cross-polarization mix time (60 us), which discriminates strongly for sites with large heteronuclear dipolar couplings and suppresses isotropic signal intensity, enables the experimental spectra to be dominated by signal intensity from the parallel and perpendicular edges of the powder patterns. It is noteworthy that the isotropic signal intensity superimposed on the powder pattern that is observed from full-length CXCR1 (WT_{1-350}) (Figure 5A and F) is significantly reduced in the corresponding spectra (Figure 5C and H) of the doubly truncated construct of CXCR1 (DT_{23-319}), which is missing the mobile N- and C- terminal residues.

This suggests that majority of the signal intensity observed around the isotropic frequency of 120 ppm in the spectra of full-length CXCR1 (WT_{1-350}) is from the mobile terminal residues.

CXCR1 in magnetically aligned bilayers

Fast rotational diffusion of membrane proteins about the bilayer normal is essential in order to obtain single line resonances from bilayers whose normals are aligned perpendicular to the direction of the applied magnetic field. Simulations show that the rotational diffusion must occur with a frequency > 10^5 per second in order to obtain narrow single line resonances (< 0.5 ppm) in the perpendicular alignment (40). Otherwise distorted or partial powder pattern line shapes are observed. We have obtained high-resolution solid-state NMR spectra of membrane proteins with between one and seven trans-membrane helices. This demonstrates that the presence of fast rotational diffusion in liquid crystalline bilayers is a property of many membrane proteins with a range of sizes, and must be taken into account in models of functional membranes. Figure 6 presented one-dimensional ^{15}N NMR spectra of uniformly ^{15}N labeled constructs of CXCR1 in aligned phospholipid bilayers.

The experimental ^{15}N solid-state NMR spectra shown in Figure 6 were obtained from full length CXCR1 (WT_{1-350}) and the doubly truncated construct DT_{23-319} in bilayers aligned with their normals perpendicular to the direction of the magnetic field. Notably, there is no evidence of powder pattern intensity in the spectra, which confirms that the proteins are aligned along with the lipids and that the proteins undergo rapid rotational diffusion about the bilayer normal. The phospholipid bilayers were well aligned as evidenced by single line ^{31}P NMR signals from the phospholipid head groups of both the short chain (DHPC) and long chain (DMPC/POPC) lipids.

Significantly, the ^{15}N NMR spectrum of doubly truncated CXCR1 (DT_{23-319}) is essentially identical to that of full-length CXCR1 (WT_{1-350}) indicating that the signals from mobile terminal residues of WT_{1-350} are not observed in aligned bilayer samples. This is consistent with previous results we have obtained on a number of smaller membrane proteins where only the signals from immobile residues were observed in the solid-state NMR spectra of magnetically aligned bilayer samples following a similar analysis (7).

The spectrum of full-length CXCR1 (WT_{1-350}) obtained with a short mix time (60 us) is dominated by signals from sites with strong heteronuclear dipolar couplings (Figure 6D), which are mostly from the trans-membrane helices (12). There are significant differences between the spectra obtained with a long mix time, which contain signals from all sites except those at the mobile termini (Figure 6A and B), and that obtained with a short mix time, which has mostly signal intensity from residues in the trans-membrane helices (Figure 6C). The simulated spectrum in Figure 6D represents the signals from the seven trans-membrane helices of a CXCR1 model structure predicted by the homology modeling program ESyPred3D (41) using the three-dimensional structure of rhodopsin (11) as a template. About half of the residues in the CXCR1 model structure are in the trans-membrane helices that are tilted by 10°-40° with respect to the membrane normal, and the comparison of the simulated spectrum in Figure 6D to the short mix experimental spectrum in Figure 6C provides confirming evidence from uniformly ^{15}N labeled samples.

Discussion

In NMR spectra the fundamental characteristics of the resonances reflect the dynamics at the sites associated with them. Consequently, the intensities, linewidths, and lineshapes of resonances can be used to describe both local and global molecular motions of proteins. By combining solution NMR and solid-state NMR experiments, a wide range of timescales can

be accessed, which enabled us to study CXCR1 in isotropic bicelles in aqueous solution and in unoriented and magnetically aligned bilayers. The solution NMR experiments on isotropic bicelle samples clearly differentiated between those residues near the N- and C-termini that undergo rapid local backbone motions and the majority of residues whose resonances are so broad due to a lack of motional averaging that they are not detectable using solution NMR experiments and instrumentation. The solid-state NMR experiments on unoriented bilayer samples confirm that some of the residues undergo substantial motional averaging because there is some isotropic intensity superimposed on the powder patterns. A variety of ^{13}C and ^{15}N NMR solid-state NMR experiments demonstrate that the CXCR1 undergoes fast rotational diffusion about the normal of liquid crystalline bilayers, but not those in the gel phase.

The conclusions about the local backbone dynamics are derived from solution NMR experiments on isotropic bicelles samples (q=0.1), and those about the global dynamics from solid-state NMR experiments performed on both magnetically aligned bilayers (q=3.2) and unoriented proteoliposomes.

The comparison between results obtained from full-length CXCR1 (WT_{1-350}) and from a construct with both the N- and C- terminal residues removed (DT_{23-319}) reinforces the conclusion that the dynamics of CXCR1 are similar to those observed in a variety of other helical membrane proteins. Essentially all membrane proteins have some mobile residues at their N- and C- termini, which show up as observable resonances in isotropic bicelles with small q values, but in q titration experiments at higher, but still isotropic phase q values it is possible to broaden all signals beyond detection. Since the 350-residue CXCR1 is a relatively large membrane protein, the discrimination between mobile and structured residues occurs at a low q of 0.1. These mobile residues either do not appear in solid-state ^{15}N NMR spectra of aligned samples, presumably because their heteronuclear dipolar couplings are too weak to enable cross-polarization, although, they do appear as relatively narrow signals near the isotropic chemical shift frequency for amide sites in unoriented samples. This spectroscopic behaviour is also typical of that we have observed in a wide variety of membrane proteins. Notably, we found no evidence of motions in the loops of CXCR1, which is also consistent with findings on other polytopic membrane proteins.

The essential dynamics of CXCR1 consist of fast local backbone motions for residues near the N- and C- termini, but not for residues in the trans-membrane helices or inter-helical loops, and rapid global rotational diffusion of the protein about the bilayer normal in liquid crystalline but not gel phase phospholipid bilayers.

Supplementary Material

Refer to Web version on PubMed Central for supplementary material.

Acknowledgments

This research was supported by grants from the National Institutes of Health, and utilized the Biomedical Technology Resource for NMR Molecular Imaging of Proteins at the University of California, San Diego, which is supported by grant P41EB002031. F.C. was supported by postdoctoral fellowships from the Swiss National Science Foundation (PBBSP3-123151) and the Novartis Foundation, formerly the Ciba-Geigy Jubilee Foundation.

References

1. Anddronesi O, Becker S, Seidel K, Heise H, Young H, Baldus M. Determiation of membrane protein structure and dyamics by magi-angle-spinning solid-state NMR spectroscopy. J Am Chem Soc. 2005; 127:12965–12974. [PubMed: 16159291]

2. Cady S, Goodman C, Tatko C, DeGrado W, Hong M. Determining the orientation of uniaxially rotating membrane proteins using unoriented samples: a H-2, C-13, and N-15 solid-state NMR investigation of the dynamics and orientation of a transmembrane helical bundle. J Am Chem Soc. 2007; 129:5719–5729. [PubMed: 17417850]

3. Leo GC, Colnago LA, Valentine KG, Opella SJ. Dynamics of fd coat protein in lipid bilayers. Biochemistry. 1987; 26:854–862. [PubMed: 3552034]

4. Bogusky MJ, Schiksnis RA, Leo GC, Opella SJ. Protein backbone dynamics by solid state and solution 15N NMR spectroscopy. J Magn Reson. 1987; 72:186–190.

5. Etzkorn M, Martell S, Andronesi OC, Seidel K, Engelhard M, Baldus M. Secondary structure, dynamics, and topology of a seven-helix receptor in native membranes, studied bby solid-state NMR spectroscopy. Angew Chem Int Ed. 2007; 46:459–462.

6. McDermott A. Structure and dynamics of membrane proeins by magic angle spinning solid-state NMR. Annu Rev Biophys. 2009; 38:385–403. [PubMed: 19245337]

7. Park SH, Das BB, DeAngelis AA, Scrima M, Opella SJ. Mechanically, Magnetically, and "Rotationally Aligned" Membrane Proteins in Phospholipid Bilayers Give Equivalent Angular Constraints for NMR Structure Determination. J Phys Chem B. 2010 in press.

8. Wylie B, Sperling L, Frericks H, Shah G, Franks W, Rienstra C. Chemical-shift anisotropy measurements of amide and carbonyl resonances in a microcrystalline protein with slow magic-angle spinning NMR spectroscopy. J Am Chem Soc. 2007; 129:5318–5319. [PubMed: 17425317]

9. Sanders, CR.; Hare, BJ.; Howard, KP.; Prestegard, JH. Progress in Nuclear Magnetic Resonance Spectroscopy. Vol. 26. 1994. Magnetically-oriented phospholipid micelles as a tool for the study of membrane-associated molecules; p. 421-444.

10. Prosser RS, Evanics F, Kitevski JL, Al-Abdul-Wahid MS. Current applications of bicelles in NMR studies of membrane-associated amphiphiles and proteins. Biochemistry. 2006; 45:8453–8465. [PubMed: 16834319]

11. Palczewski K, Kumasaka T, Hori T, Behnke CA, Motoshima H, Fox BA, Le Trong I, Teller DC, Okada T, Stenkamp RE, Yamamoto M, Miyano M. Crystal structure of rhodopsin: A G protein-coupled receptor. Science. 2000; 289:739–745. [PubMed: 10926528]

12. Park SH, Prytulla S, De Angelis AA, Brown JM, Kiefer H, Opella SJ. High-resolution NMR spectroscopy of a GPCR in aligned bicelles. J Am Chem Soc. 2006; 128:7402–7403. [PubMed: 16756269]

13. Clubb RT, Omichinski JG, Clore GM, Gronenborn AM. Mapping the binding surface of interleukin-8 complexed with an N-terminal fragment of the type 1 human interleukin-8 receptor. FEBS Lett. 1994; 338:93–97. [PubMed: 8307164]

14. Ravindran A, Joseph PR, Rajarathnam K. Structural basis for differential binding of the interleukin-8 monomer and dimer to the CXCR1 N-domain: role of coupled interactions and dynamics. Biochemistry. 2009; 48:8795–8805. [PubMed: 19681642]

15. Loetscher P, Seitz M, Clark-Lewis I, Baggiolini M, Moser B. Both interleukin-8 receptors independently mediate chemotaxis. Jurkat cells transfected with IL-8R1 or IL-8R2 migrate in response to IL-8, GRO alpha and NAP-2. FEBS Lett. 1994; 341:187–192. [PubMed: 8137938]

16. Fu W, Zhang Y, Zhang J, Chen WF. Cloning and characterization of mouse homolog of the CXC chemokine receptor CXCR1. Cytokine. 2005; 31:9–17. [PubMed: 15967374]

17. Skrabanek L, Campagne F, Weinstein H. Building protein diagrams on the web with the residue-based diagram editor RbDe. Nucleic Acids Res. 2003; 31:3856–3858. [PubMed: 12824436]

18. Degrip WJ, Vanoostrum J, Bovee-Geurts PH. Selective detergent-extraction from mixed detergent/lipid/protein micelles, using cyclodextrin inclusion compounds: a novel generic approach for the preparation of proteoliposomes. Biochem J. 1998; 330(Pt 2):667–674. [PubMed: 9480873]

19. Signorell GA, Kaufmann TC, Kukulski W, Engel A, Remigy HW. Controlled 2D crystallization of membrane proteins using methyl-b-cyclodextrin. Journal of Structural Biology. 2007; 157:321–328. [PubMed: 16979348]

20. De Angelis AA, Opella SJ. Bicelle samples for solid-state NMR of membrane proteins. Nat Protoc. 2007; 2:2332–2338. [PubMed: 17947974]

21. Mori S, Abeygunawardana C, Johnson MO, van Zijl PC. Improved sensitivity of HSQC spectra of exchanging protons at short interscan delays using a new fast HSQC (FHSQC) detection scheme that avoids water saturation. J Magn Reson B. 1995; 108:94–98. [PubMed: 7627436]
22. Palmer AG, Cavanagh J, Wright PE, Rance M. Sensitivity improvement in proton-detected two-dimensional heteronuclear correlation NMR spectroscopy. Journal of Magnetic Resonance (1969). 1991; 93:151–170.
23. Grzesiek S, Bax A. Improved 3D triple-resonance NMR techniques applied to a 31 kDa protein. Journal of Magnetic Resonance (1969). 1992; 96:432–440.
24. Levitt MH, Suter D, Ernst RR. Spin dynamics and thermodynamics in solid-state NMR cross polarization. J Chem Phys. 1986; 84:4243.
25. Yu Y, Fung BM. An efficient broadband decoupling sequence for liquid crystals. J Magn Reson. 1998; 130:317–320. [PubMed: 9500905]
26. Liu SF, Mao JD, Schmidt-Rohr K. A robust technique for two-dimensional separation of undistorted chemical-shift anisotropy powder patterns in magic-angle-spinning NMR. J Magn Reson. 2002; 155:15–28. [PubMed: 11945029]
27. States DJ, Haberkorn RA, Ruben DJ. A two-dimensional nuclear overhauser experiment with pure absorption phase in four quadrants. Journal of Magnetic Resonance (1969). 1982; 48:286–292.
28. Amman C, Meier P, Merbach AE. A Simple Multinuclear Thermometer. J Magn Reson. 1982; 46:319–321.
29. Bak M, Rasmussen JT, Nielsen NC. SIMPSON: a general simulation program for solid-state NMR spectroscopy. J Magn Reson. 2000; 147:296–330. [PubMed: 11097821]
30. Grant CV, Yang Y, Glibowicka M, Wu CH, Park SH, Deber CM, Opella SJ. A Modified Alderman-Grant Coil makes possible an efficient cross-coil probe for high field solid-state NMR of lossy biological samples. J Magn Reson. 2009; 201:87–92. [PubMed: 19733108]
31. Delaglio F, Grzesiek S, Vuister GW, Zhu G, Pfeifer J, Bax A. NMRPipe: a multidimensional spectral processing system based on UNIX pipes. J Biomol NMR. 1995; 6:277–293. [PubMed: 8520220]
32. Van Horn WD, Kim HJ, Ellis CD, Hadziselimovic A, Sulistijo ES, Karra MD, Tian C, Sonnichsen FD, Sanders CR. Solution nuclear magnetic resonance structure of membrane-integral diacylglycerol kinase. Science. 2009; 324:1726–1729. [PubMed: 19556511]
33. Gautier A, Mott HR, Bostock MJ, Kirkpatrick JP, Nietlispach D. Structure determination of the seven-helix transmembrane receptor sensory rhodopsin II by solution NMR spectroscopy. Nat Struct Mol Biol. 2010; 17:768–774. [PubMed: 20512150]
34. Goncalves, JA.; Ahuja, S.; Erfani, S.; Eilers, M.; Smith, SO. Progress in Nuclear Magnetic Resonance Spectroscopy. Vol. 57. 2010. Structure and function of G protein-coupled receptors using NMR spectroscopy; p. 159-180.
35. Tian C, Breyer RM, Kim HJ, Karra MD, Friedman DB, Karpay A, Sanders CR. Solution NMR spectroscopy of the human vasopressin V2 receptor, a G protein-coupled receptor. J Am Chem Soc. 2005; 127:8010–8011. [PubMed: 15926814]
36. Pervushin K, Riek R, Wider G, Wuthrich K. Attenuated T2 relaxation by mutual cancellation of dipole-dipole coupling and chemical shift anisotropy indicates an avenue to NMR structures of very large biological macromolecules in solution. Proc Natl Acad Sci U S A. 1997; 94:12366–12371. [PubMed: 9356455]
37. Lewis BA, Harbison GS, Herzfeld J, Griffin RG. NMR structural analysis of a membrane protein: bacteriorhodopsin peptide backbone orientation and motion. Biochemistry. 1985; 24:4671–4679. [PubMed: 4063350]
38. Herzfeld J, Berger AE. Sideband intensities in NMR spectra of samples spinning at the magic angle. J Chem Phys. 1980; 73:6021–6030.
39. de Dios AC, Laws DD, Oldfield E. Predicting Carbon-13 Nuclear Magnetic Resonance Chemical Shielding Tensors in Zwitterionic L-Threonine and L-Tyrosine via Quantum Chemistry. J Am Chem Soc. 1994; 116:7784–7786.
40. Nevzorov, AA.; De Angelis, AA.; Park, SH.; Opella, SJ. Uniaxial motional averaging of the chemical shift anisotropy of membrane proteins in bilayer environments. In: Ramamoorthy, A., editor. NMR Sectroscopy of Biological Solids. Marcel Dekker; New York: 2005. p. 173-184.

41. Lambert C, Leonard N, De Bolle X, Depiereux E. ESyPred3D: Prediction of proteins 3D structures. Bioinformatics. 2002; 18:1250–1256. [PubMed: 12217917]

Abbreviations

$3TM_{193-350}$	C-terminal 3 transmembrane CXCR1
CT_{1-319}	C-terminal truncated CXCR1
DT_{23-319}	doubly N- and C-terminal truncated CXCR1
MAS	magic angle spinning
ND_{1-38}	N-terminal domain of CXCR1
NT_{39-350}	N-terminal truncated CXCR1
WT_{1-350}	wild-type CXCR1
DHPC	1,2-dihexanoyl-sn-glycero-3-phosphocholine
DMPC	1,2-dimyristoyl-sn-glycero-3-phosphocholine
GST	glutathione S-transferase
TCEP	tris-2-carboxyethyl-phosphine

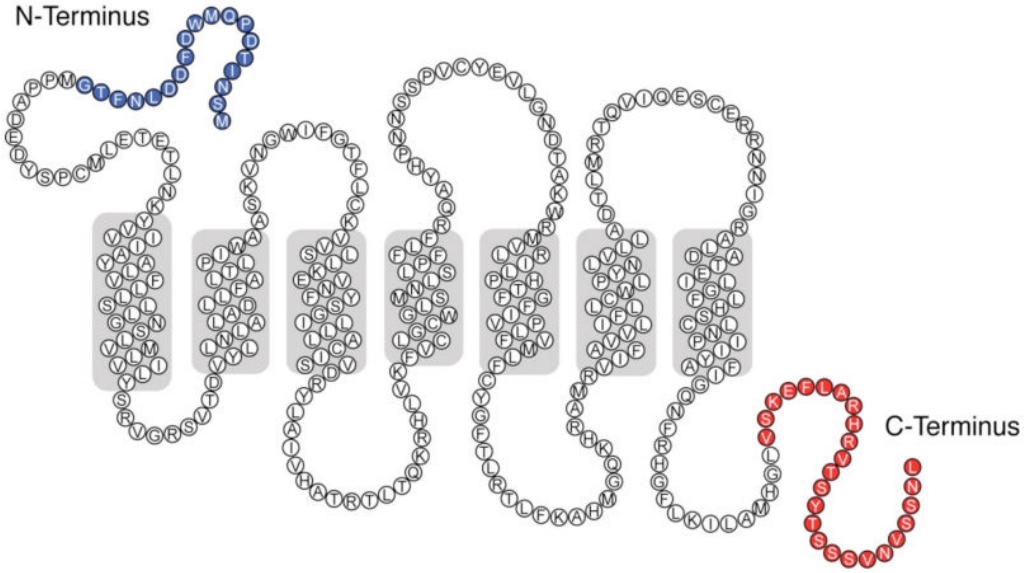

Figure 1.

Representation of the amino acid sequence of CXCR1 arranged to show the trans-membrane helices, inter-helical loops, and terminal regions predicted by a hydropathy analysis. The N- and C-terminal residues found to be mobile by the NMR experiments are colored in blue and red, respectively.

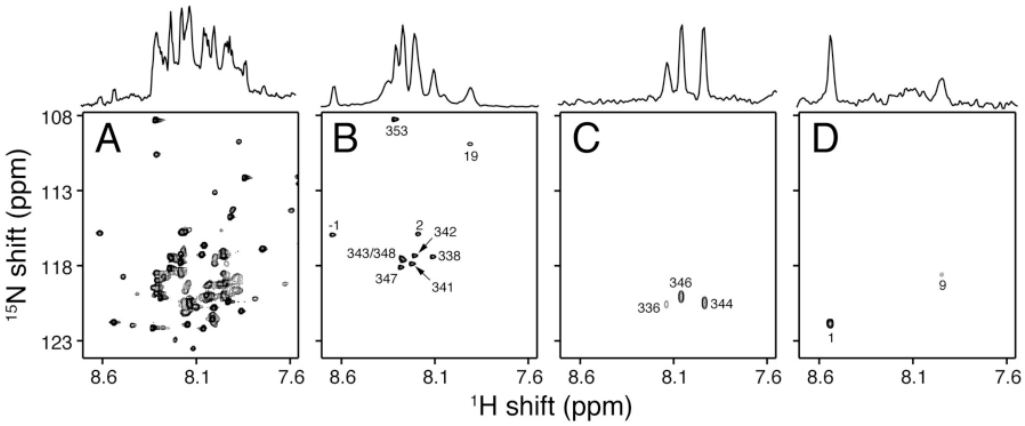

Figure 2.

Experimental solution $^{1}H/^{15}N$ HSQC NMR spectra of uniformly and selectively ^{15}N labeled full-length CXCR1 (WT_{1-350}) in q=0.1 isotropic bicelles at 50°C. (A) Uniformly ^{15}N labeled. (B) Selectively ^{15}N glycine and serine labeled. (C) Selectively ^{15}N valine labeled. (D) Selectively ^{15}N methionine labeled. The assignments of the amide resonances are marked by residue numbers.

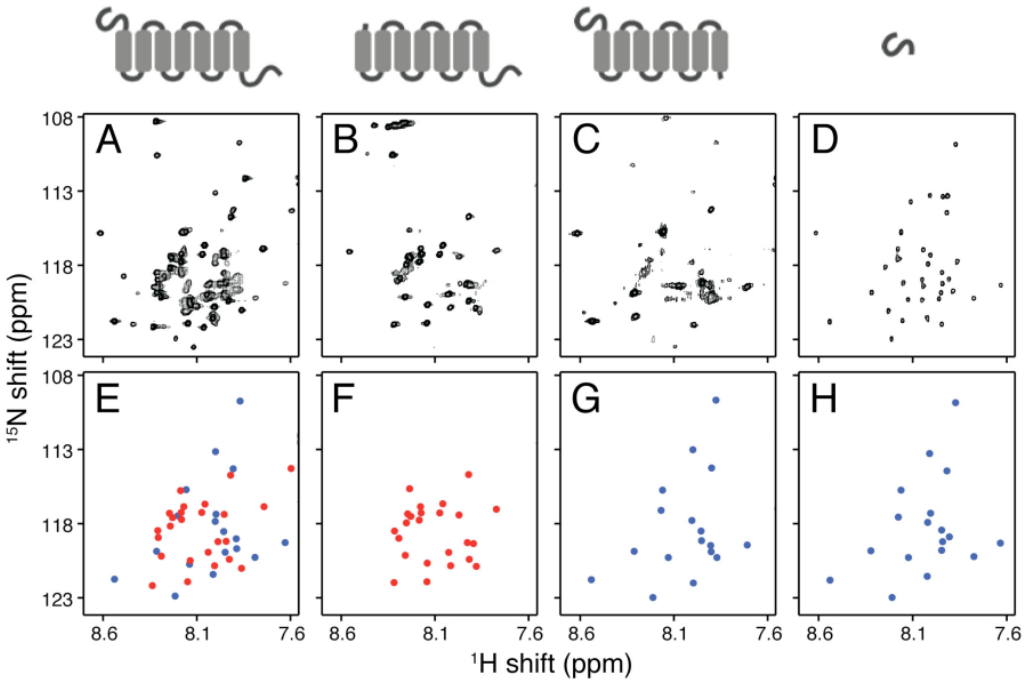

Figure 3.

Experimental solution $^{1}H/^{15}N$ HSQC NMR spectra of uniformly ^{15}N labeled CXCR1 constructs in q=0.1 isotropic bicelles at 50°C. (A) Full-length CXCR1 (WT_{1-350}). (B) N-terminal truncated CXCR1 (NT_{39-350}). (C) C-terminal truncated CXCR1 (CT_{1-319}). (D) N-terminal domain (ND_{1-38}). (E – H) Colored "dot" representations of the experimental solution NMR spectra above that facilitate comparisons among the various constructs of CXCR1. Blue dots correspond to resonances assigned to mobile residues at the N-terminus. Red dots correspond to resonances assigned to mobile residues at the C-terminus. Unassigned signals are from the extra residues added to enable the expression, enzymatic cleavage and purification of the receptors (see supplemental information).

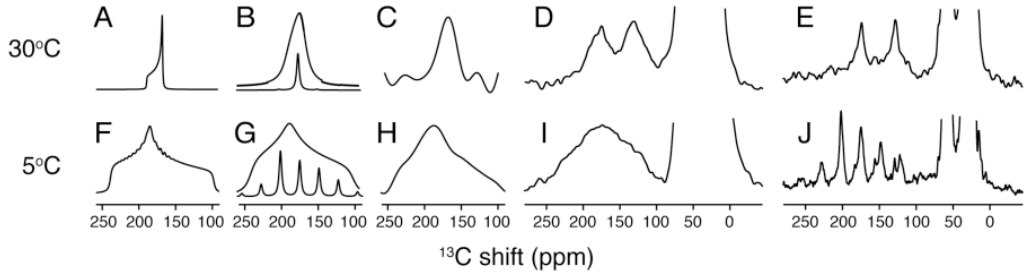

Figure 4.

Solid-state ^{13}C NMR spectra of uniformly 35% ^{13}C, 100% ^{15}N labeled full-length CXCR1 (WT_{1-350}) in unoriented DMPC/POPC bilayers. (A – E) The experiments were performed at 30°C where CXCR1 undergoes fast rotational diffusion about the bilayer normal. (F – J) The experiments were performed at 5°C where CXCR1 is immobile. (A and F) Simulated carbonyl ^{13}C chemical shift powder patterns for a residue in a trans-membrane helix with 200 Hz of added line broadening. (B and G) Simulated MAS solid-state NMR spectra as in (A) with 200 Hz and 3 kHz, respectively, of added line broadening. (C and H) Experimental MAS solid-state ^{13}C NMR spectra of carbonyl powder patterns obtained with the two-dimensional SUPER CSA recoupling experiment; the spinning rate was 5 kHz. (D and I) Experimental solid-state ^{13}C NMR chemical shift powder patterns obtained from a stationary sample. (E and J) Experimental MAS ^{13}C NMR spectra; the spinning rate was 5 kHz.

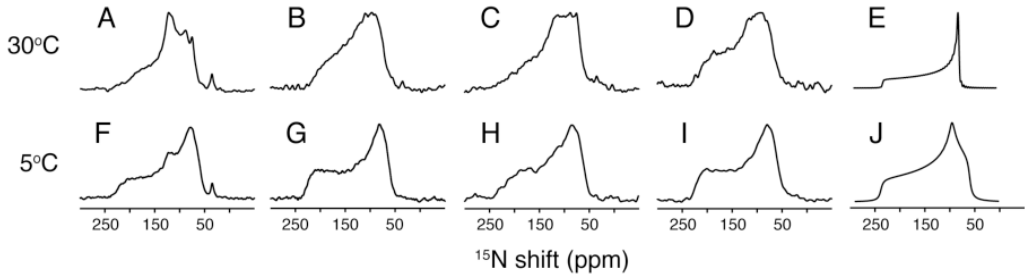

Figure 5.

Solid-state ^{15}N NMR spectra of uniformly ^{15}N labeled full-length CXCR1 (WT_{1-350}) and doubly truncated CXCR1 (DT_{23-319}) in unoriented DMPC/POPC bilayers. (A – D) The experiments were performed at 30°C where CXCR1 undergoes fast rotational diffusion about the bilayer normal. (E – H) The experiments were performed at 5°C where CXCR1 is immobile. The spectra were obtained with a long (1 ms) (A, C, F, and H) and a short (60 μs) (B, D, G, and I) cross-polarization mix time. (E) Simulated ^{15}N amide chemical shift powder pattern for a residue in a trans-membrane helix undergoing fast rotational diffusion about the bilayer normal. (J) Simulated ^{15}N amide chemical shift powder pattern for an immobile site. The simulations utilized principal values of σ_{11} = 64 ppm, σ_{22} = 92 ppm, σ_{33} = 234 ppm, and isotropic value of σ_{iso} = 120 ppm.

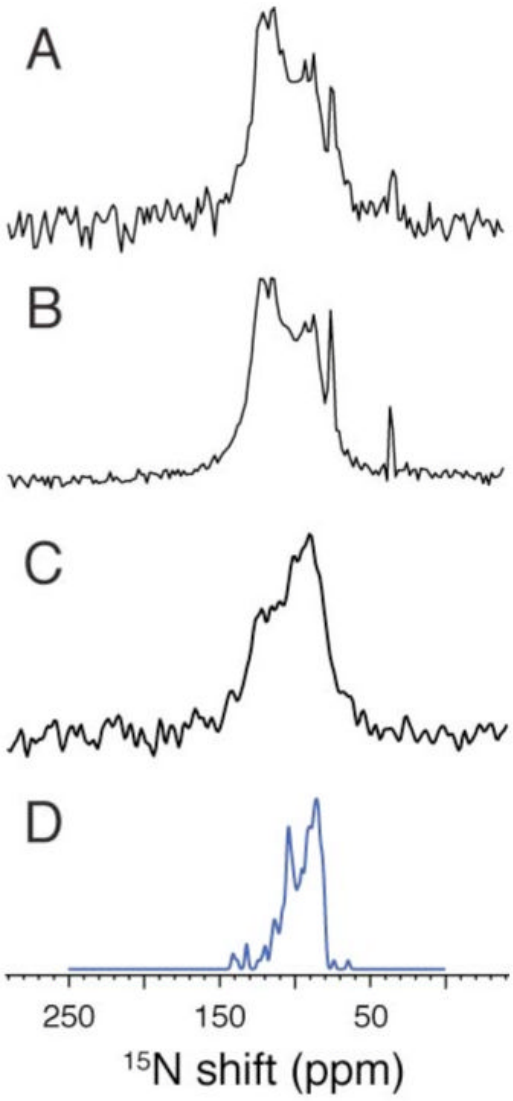

Figure 6.

Solid-state ^{15}N NMR spectra of uniformly ^{15}N labeled full-length CXCR1 (WT_{1-350}) and doubly truncated CXCR1 (DT_{23-319}) in magnetically aligned DHPC: DMPC/POPC bilayers (q=3.2) at 30°C; the bilayer normals are perpendicular to the applied magnetic field. (A) Full-length CXCR1 (WT_{1-350}) spectrum obtained with a long (1 ms) cross-polarization mix time. (B) Doubly truncated CXCR1 (DT_{23-319}) spectrum obtained with a long (1 ms) cross-polarization mix time. (C) Full-length CXCR1 (WT_{1-350}) spectrum obtained with a short (60 μs) cross-polarization mix time. (D) Simulated ^{15}N NMR spectrum of the trans-membrane helices of uniformly ^{15}N labeled CXCR1 based on a calculated model structure.